A Mode Switching Sliding-mode Controller with Observer-based State-Dependent Boundary Layer and Its Application

Liang-Chun Yao d917701@oz.nthu.edu.tw
Department of Power Mechanical Engineering
National Tsing-Hua University
HsinChu, 30013, Taiwan

Jian-Shiang Chen jschen@pme.nthu.edu.tw
Department of Power Mechanical Engineering
National Tsing-Hua University
HsinChu, 30013, Taiwan

Chao-Yu Hsu g913760@oz.nthu.edu.tw
Department of Power Mechanical Engineering
National Tsing-Hua University
HsinChu, 30013, Taiwan

Abstract

This paper presents a mode-switching sliding-mode control (MSMC) scheme that combines different sliding-mode control schemes to alleviate adverse effect while achieving precise control tasks. To achieve certain robustness and chattering alleviation, a design of disturbance observer based state-dependent boundary layer is proposed. The proposed method will provide a state-dependent boundary-layer in which the unknown dynamics is estimated a disturbance observer and then utilize it to calculate the width of boundary layer on-line. The convergent analysis of this state-dependent boundary-layer is provided with two theorems. Finally, its efficacy is further validated through experiments on the regulation control of a maglev platform.

Keywords: sliding mode, mode-switching, boundary layer, maglev platform.

1. INTRODUCTION

Sliding mode control (SMC), a high-speed switching feedback control methodology, has received much attention both in theory and applications for the last decades. Generally, one of its salient features is known to be its robustness against uncertainties both in system parameters and dynamics [1][2]. However, one of the major drawbacks of the sliding mode control is the adverse chatters while the controller input undergoes very fast activity of switching [3]. Nevertheless most SMC designs prove its efficacy in maintaining both stability and robust performance in counteracting modeling imprecision and external disturbances as well. The chatters can always be alleviated by the *so-called* boundary layer approach [4], in which the discontinuous control activity is replaced by a continuous control effort inside a preset boundary layer around the switching surface. However, its robust performance would inevitably be deteriorated with this augmented boundary-layer. In general, the layer thickness or width is either fixed or time

invariant, tradeoffs between alleviated chatters and robust performance could highly depend on the choice of layer thickness. Physically speaking, the boundary layer can be approximated as a low-pass filter for a high frequency switching output, the cut-off frequency of this filter would be very difficult to be determined, however. In [5], the controller design adopted physical properties of a robot manipulator and a set of time-varying switching gains and boundary layer are incorporated in the sliding mode controller to accelerate the state trajectories moving toward the sliding hyper-plane, the design turned out to be much complicated and the system dynamics must be known as a *priori.*

A state-dependent boundary layer approach were proposed by [6][7], in which the thickness of boundary layer can be adjusted online based-on the state norm for a class of uncertain linear systems. On the other hand, aimed at nonlinear systems, a mode-switching control (MSC) scheme is usually adopted to improve the accuracy and robustness of controller design. In [8], Iwasaki, Sakai and Matsui applied the MSC in a two-degree-of -freedom position control system to achieve both fast response and high accuracy. And Takashi, Hidehiko and Hiromu [9] proposed the MSC with initial value compensation to determine the optimal switching conditions for the disk drives. In[10], different SMC schemes based on mode switching was reported, it is noted that difficulties were encountered in the compromising between compatibility and robustness while mode switching took place.

The SMC design provides an effective approach in maintaining stability and robust performance due to modeling imprecision. However, the performance of controller will be deteriorated with augmented boundary-layer approach, and the steady-state error will occur. The integral SMC can reduce the steady-state error and chattering as compared to boundary-layer approach, but the additional integral term could cause the actuator's windup. This paper is aimed to propose a mode-switching sliding-mode control (MSMC) scheme that combines different SMC schemes to alleviate adverse effect while achieving precise control task. Here, both compatibility and robustness are resolved by a disturbance observer based state-dependent boundary layer design incorporated with MSMC is proposed. This proposed scheme can estimate uncertainties by a disturbance observer and then utilize it to calculate the thickness/width of the boundary layer on-line. Finally, to demonstrate the efficacy and feasibility of the proposed method, a maglev platform is devised to validate the proposed schemes through experiment studies.

2. PROBLEM STATEMENT

Consider an uncertain SISO system with matched uncertainties [10] and described as

$$q^{(n)} = f(t,\boldsymbol{q}) + b(t,\boldsymbol{q})u + d \tag{1}$$

where q is the output, u is the control input, and $\boldsymbol{q} = [q \;\; \dot{q} \cdots q^{(n-1)}]^T$ is the corresponding state vector. $b(t,\boldsymbol{q})$ is a non-zero function and of known sign as a *priori*. $f(t,\boldsymbol{q})$ and $b(t,\boldsymbol{q})$ are bounded uncertain functions, d is bounded disturbance and satisfies the following inequalities.

$$\left|f(t,q) - \bar{f}(t,q)\right| \le F;\ \left|b(t,q) - \bar{b}(t,q)\right| \le B;\ \left|d\right| \le D \tag{2}$$

Where $\bar{f}(t,\boldsymbol{q})$ and $\bar{b}(t,\boldsymbol{q})$ are nominal functions. If we further assume that $\boldsymbol{q_d}$ is the command vector to be tracked, and its initial state vector is known as $\boldsymbol{q_d(0)=q(0)}$. We can then define $\tilde{\boldsymbol{q}} = \boldsymbol{q} - \boldsymbol{q_d}$ to be the tracking error, thus $\tilde{\boldsymbol{q}} = \boldsymbol{q} - \boldsymbol{q_d} = [\tilde{q} \;\; \dot{\tilde{q}} \cdots \tilde{q}^{(n-1)}]^T$ being the tracking error vector.

Lemma 1 Slotine(1983)[5]:
A time-varying surface *s(t)* defined in $\mathbf{R}^{(n)}$ can be defined by a scalar equation $s(\tilde{q},t)=0$ and shown as below

$$s(\tilde{q},t)=(\frac{d}{dt}+\lambda)^{n-1}\tilde{q} \tag{3}$$

In which λ is a positive constant. Furthermore, bounds on *s* can be directly related to bounds on the tracking error vector $\tilde{q}$, therefore $s(\tilde{q},t)$ represents a true measure of the tracking performance. Specifically, assuming $\tilde{q}(0)=\mathbf{0}$, the bound of tracking error can be written as

$$\left|\tilde{q}^{(i)}(t)\right| \le (2\lambda)^i \varepsilon \quad i=0,1,...,n-1;\ \forall t \ge 0 \tag{4}$$

where $\varepsilon=\Phi/\lambda^{n-1}$ is the boundary layer width.

Lemma 2 Slotine(1983)[5]:
To reduce chatters induced by imperfect switching, the discontinuous control can be approximated inside a boundary layer located around the switching surface, while Φ , the thickness of the boundary layer is state-dependent or time-varying and a filtered output of a pre-specified trajectory $k(\boldsymbol{q}_d)$ and sliding motion is asymptotically stable. And,

$$s\dot{s} \le \left(\dot{\Phi}-\eta\right)|s| \tag{5}$$

$$\dot{\Phi}+\lambda\Phi=k\left(\boldsymbol{q}_d\right) \tag{6}$$

Supposed that we wish to design a sliding-mode control system with at least two sliding surfaces and both accompany with state-dependent boundary layer, a Mode-Switching Control scheme is thus augmented to achieve fast transient response, less chatters with better robustness. Without the loss of generality, we consider the switching between two sliding-mode schemes, e.g. a sliding-mode control (SMC) scheme and an integral sliding-mode control (ISMC) scheme, they are depicted as follows.

$$\begin{cases} s=(\frac{d}{dt}+\lambda)^{n-1}\tilde{q} & |s|\ge\Phi \\ s_I=(\frac{d}{dt}+\lambda_I)^n\int_0^t \tilde{q}dt & |s_I|<\Phi \end{cases} \tag{7}$$

Here *s* and s_I are the sliding variables, $\tilde{q}=q-q_d$, *q* is the generalized coordinate, q_d is the desired output; Φ is the pre-specified layer thickness, while λ and λ_I are the corresponding eigenvalues of the sliding mode control and integral sliding mode control, respectively. From (3), for *n*=2 we will have the following estimates of the bounds ε and ε_I on errors,

$$\varepsilon=\frac{\Phi}{\lambda} \text{ and } \varepsilon_I=\frac{\Phi}{2\lambda_I} \tag{8}$$

If $2\lambda_I \le \lambda$, ε will be equal to or less than ε_I which implies that one cannot ensure ISMC will t switching back to SMC, while $2\lambda_I > \lambda$, ISMC will converge to $0<|\tilde{q}|<\varepsilon_I$ provided that no disturbance is encounter. Consequently, It is concluded that if $\lambda \ne 2\lambda_I$, sliding variable will encounter compatibility problem while switching occurs between $|s|<\Phi$ and $|s_I|>\Phi$. Instead of switching based on the sliding variable, for *n*=2, the mode-switching condition needs to be modified as follows [9].

$$s=\begin{cases} \dot{\tilde{q}}+\lambda\tilde{q} \\ \dot{\tilde{q}}+2\lambda_I\tilde{q}+\lambda_I^2\int_{t_s}^t \tilde{q}dt \end{cases} \text{ switching at } t_s \text{ and } |\tilde{q}|=\varepsilon \tag{9}$$

Here t_s is the pre-specified time of switching, $\varepsilon=\Phi/\lambda$ is the pre-specified layer width while switching occurs. The choice of thickness will affect the robustness As described by [7], a state-dependent boundary layer control is capable of ensuring effective chattering alleviation with state-

dependent uncertainties but the adverse effect of external disturbances still exist, in other words, ineffective switching might occur on (9) without a better estimation on the bounds of disturbances.

3. A STATE-DEPENDNET BOUNDARY LAYER WITH DISTURBANCE OBSERVER

As shown in Fig. 1, consider the dynamic system as described in (1), we wish to track a desired command $\boldsymbol{q_d(t)}$, a pole-placement design using feedback-linearization technique leads to the following control law[11].

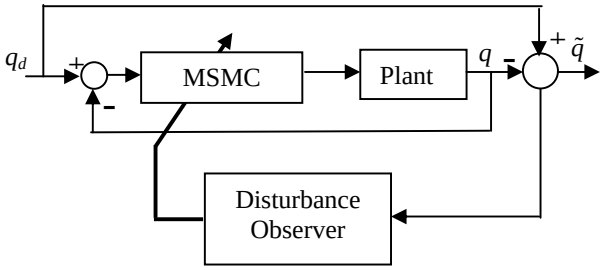

FIGURE 1: Block diagram of the proposed controller with disturbance observer

$$u = u_{pa} = \frac{1}{\hat{b}(t,q)}[-\hat{f}(t,q) + q_d^{(n)} - \sum_{i=0}^{n-1} c_i \tilde{q}^{(n)}] \tag{10}$$

in which u_{pa} represents the control effort using the design in Eq.(9); $\hat{f}(t,\mathbf{q})$ and $\hat{b}(t,\mathbf{q})$ are the estimates of functions $f(t,\boldsymbol{q})$ and $b(t,\boldsymbol{q})$, respectively. With $p \equiv d/dt$, the coefficients, c_i, i = 0, 1, 2,…, n-1, of the desired characteristic equation are rewritten as

$$p^n + c_{n-1}p^{n-1} + c_{n-2}p^{n-2} + \cdots + c_1 p + c_0 = 0 \tag{11}$$

has the desired multiple roots, at $-\lambda$, leading to a desired exponentially stable error dynamics. And,

$$\tilde{q}^{(n)} + c_{n-1}\tilde{q}^{(n-1)} + c_{n-2}\tilde{q}^{(n-2)} + \cdots + c_1\dot{\tilde{q}} + c_0\tilde{q} = 0 \tag{12}$$

provided that the bounded uncertainties, d vanishes and the nominal functions, $\hat{f}(t,\mathbf{q})$ and $\hat{b}(t,\mathbf{q})$ would coincide with $f(t,\boldsymbol{q})$ and $b(t,\boldsymbol{q})$. However, perturbation often arises and causes the resultant error dynamics to deviate from the desired one in an adverse way.

This effect can be revealed further by manipulating Eq. (1) and substituting the control law, Eq. (10) to yield

$$q^{(n)} = q_d^{(n)} - \sum_{i=0}^{n-1} c_i \tilde{q}^{(i)} + [f(t,q) - \hat{f}(t,q)] + [b(t,q) - \hat{b}(t,q)]u + d \tag{13}$$

Rearranging Eq.(13) to yield,

$$\tilde{q}^{(n)} + c_{n-1}\tilde{q}^{(n-1)} + c_{n-2}\tilde{q}^{(n-2)} + \cdots + c_1\dot{\tilde{q}} + c_0\tilde{q} = \psi \tag{14}$$

where $\psi = \left(f(t,q) - \hat{f}(t,q)\right) + \left(b(t,q) - \hat{b}(t,q)\right)u + d(t)$ is noted as a *lumped-perturbation* in the

controller design and may cause an undesirable overshoot or, more severely, system instability. To compensate for the perturbation, the control law from Eq.(10) is redesigned with an extra compensation term, i.e.

$$u=u_{pa}+u_{pc} \tag{15}$$

Consequently, Eq.(1) becomes

$$q^{(n)} = q_d^{(n)} - \sum_{i=0}^{n-1} c_i \tilde{q}^{(i)} + \hat{b}(t,q)u_{pc} + \psi \tag{16}$$

To compensate for ψ , we would like to have $\hat{b}(t,q)u_{pc} = -\hat{\psi}$ to yield

$$q^{(n)} = q_d^{(n)} - \sum_{i=0}^{n-1} c_i \tilde{q}^{(i)} + \psi - \hat{\psi} \tag{17}$$

Ideally, $\hat{\psi}$ should be set equal to ψ , then the error dynamics would follow Eq.(12). To obtain the estimate of the perturbation, $\hat{\psi}$, an auxiliary process is adopted and defined as

$$\dot{w} = q_d^{(n)} - \sum_{i=0}^{n-1} c_i \tilde{q}^{(i)} + \hat{b}(t,q)u_{pc} + \Psi \operatorname{sgn}(\sigma_q) \tag{18}$$

And, based on Eq.(2), we have

$$\Psi = -\left[F(t,q) + B(t,q)|u| + D(t)\right]$$

Furthermore, a switching function is defined as

$$\sigma_q = q^{(n-1)} - w \tag{19}$$

Without the loss of generality, we adopted the case in Eq.(9), for the switching of two different SMCs, we should have the following auxiliary process,

$$\dot{w} = \begin{cases} \ddot{q}_d - \lambda_q \dot{\tilde{q}} + \Psi \operatorname{sgn}(\sigma_q) - \hat{\psi}_1 & |\tilde{q}| > \varepsilon_q \\ \ddot{q}_d - 2\lambda_q \dot{\tilde{q}} - \lambda_q^2 \tilde{q} + \Psi \operatorname{sgn}(\sigma_q) - \hat{\psi}_2 & |\tilde{q}| \le \varepsilon_q \end{cases} \tag{20}$$

Here, $\hat{\psi}_1$ and $\hat{\psi}_2$ are perturbations estimated for ψ_1 and ψ_2 , respectively.

Theorem 1:
Let $\hat{\psi}_1$ and $\hat{\psi}_2$ be defined as in Eq.(20), and

$$\hat{\psi} = \hat{\psi}_1 + \hat{\psi}_2 \tag{21}$$

A sliding function with n=2 in (19) that defined a global sliding mode is established using auxiliary process as described in Eq.(20). And let $\hat{\psi}_1$ and $\hat{\psi}_2$ be estimated from the following,

$$\dot{\hat{\psi}}_1 = K_{c1}\Psi \operatorname{sgn}(\sigma_q) \tag{22}$$

$$\dot{\hat{\psi}}_2 = -K_{c2}\psi_2 + K_{c2}\Psi \operatorname{sgn}(\sigma_q) \tag{23}$$

where K_{c1} and K_{c2} are constants to be determined based on the range of bandwidth of interest. Then, we have an invariant condition

$$\frac{\hat{\psi}(p)}{\psi(p)} = \frac{(K_{c2}+K_{c1})p + K_{c2}K_{c1}}{(p+K_{c2})(p+K_{c1})} \tag{24}$$

Proof:

From Eq.(19), with n=2, we have

$$\dot{\sigma}_q = \ddot{q} - \dot{w} = \psi - \hat{\psi} - \Psi \operatorname{sgn}(\sigma_q) + \hat{\psi}_2 = \psi - \hat{\psi}_1 - \Psi \operatorname{sgn}(\sigma_q) \tag{25}$$

with $\dot{\sigma}_q = 0$, we could find

$$\frac{\hat{\psi}_1(p)}{\psi(p)} = \frac{K_{c1}}{p + K_{c1}}$$

and $$\frac{\hat{\psi}_2(p)}{\psi(p)} = \frac{K_{c2} p}{(p + K_{c1})(p + K_{c2})}$$

Therefore,

$$\frac{\hat{\psi}(p)}{\psi(p)} = \frac{(K_{c2} + K_{c1}) p + K_{c2} K_{c1}}{(p + K_{c2})(p + K_{c1})}$$

■

This relationship is invariant to variations of system parameters, and the estimate $\hat{\psi}$ is intrinsically a low-pass-filtered version of disturbance ψ with the filter's bandwidth determined by the constants K_{c1} and K_{c2}. Ideally, $\hat{\psi}$ should be set equal to ψ. Increasing the value of K_{c1} and K_{c2} approaches this ideal case, improves the effectiveness of disturbance compensation, but may increase the chatter level in control input. As a rule of thumb, the filter's bandwidth is usually chosen to be about ten times that of the closed-loop system, that is, $K_{c1} = K_{c2} = 10\omega_n$.

Remark1:
w is the state variable of the auxiliary process, the switching function σ_q is defined as (19) and the switching gain Ψ is assigned so that $\left|\psi - \hat{\psi}_1\right| < \Psi$. Here, $\operatorname{sgn}(\cdot)$ denotes the sign function. To ensure a sliding regime $\sigma_q = 0$, the sliding condition

$$\lim_{\sigma_q \to 0} \sigma_q \dot{\sigma}_q < 0$$

should be satisfied. Consideration here of Lyapunov candidate $V = 0.5\sigma_q^2$. Taking the derivative *V* with respect to time and substituting (20), (17) and (25) into the resulting equation gives. Multiplying both sides of (25) by σ_q and noting that $\left|\psi - \hat{\psi}_1\right| < \Psi$, we have

$$\dot{V} = \sigma_q \dot{\sigma}_q = \left(\psi - \hat{\psi}_1\right)\sigma_q - \Psi\left|\sigma_q\right| < 0, \qquad \text{if } \sigma_q \neq 0$$

which implies the satisfaction of the sliding condition and the existence of the sliding regime $\sigma_q = 0$ after some time. Subsequently, assigning the initial state of the auxiliary process as

$$w(t = 0) = \dot{q}(t = 0)$$

gives $\sigma_q = 0$ at $t = 0$.
This together with the satisfaction of the sliding condition implies that $\sigma_q = 0$ for all $t \geq 0$.
Thus, the sliding regime $\sigma_q = 0$ exists for the disturbance estimation during an entire response despite the presence of system disturbance which is desired to be estimated.

Theorem 2

Assuming that boundary layer Φ can be determined based on the lumped disturbance estimated by $\hat{\psi}$, and Eq.(6) is rewritten as

$$\dot{\Phi} + \lambda_{\Phi}\Phi = \hat{\psi} \tag{26}$$

Then, the bandwidth of state-dependent boundary layer can be chosen accordingly, i.e.

$$\lambda_{\Phi} = \frac{K_{c2}K_{c1}}{K_{c2} + K_{c1}} \tag{27}$$

And, the state-dependent boundary layer with observer is bounded and a quasi-sliding mode is assured.

Proof:

From Eq.(26) and Eq.(24), we have

$$\Phi(p) = \frac{1}{p + \lambda_{\Phi}}\hat{\psi}(p) \tag{28}$$

$$\hat{\psi}(p) = \frac{(K_{c2} + K_{c1})p + K_{c2}K_{c1}}{(p + K_{c2})(p + K_{c1})}\psi(p) \tag{29}$$

Combine (27) and (28) to yield

$$\Phi(p) = \frac{(K_{c2} + K_{c1})\left(p + \frac{K_{c2}K_{c1}}{K_{c2} + K_{c1}}\right)}{(p + \lambda_{\Phi})(p + K_{c2})(p + K_{c1})}\psi(p) \tag{30}$$

Consequently, using $\lambda_{\Phi} = \frac{K_{c2}K_{c1}}{K_{c2} + K_{c1}}$, Eq. (30) is reduced to

$$\frac{\Phi(p)}{\psi(p)} = \frac{(K_{c2} + K_{c1})}{(p + K_{c2})(p + K_{c1})} \tag{31}$$

Since K_{c1} and K_{c2} are positive constants, if the perturbation is bounded, then the state-dependent boundary based on disturbance observer is bounded and asymptotically stable is assured.

Remark2: The thickness of boundary layer $\Phi(p)$ is the filter output of the system perturbation ψ through an over-damped second order low-pass filter with pre-specified bandwidth. Accordingly, even if ψ is with high-frequency content or with discontinuous jump, only low-frequency part of Φ will be preserved. Furthermore, ψ can be estimated from $\hat{\psi}$, and a bounded Φ is assured.

4. EXPERIMENTAL STUDIES

The Experimental Setup [10]

As shown in Fig. 2, a two-D.O.F maglev platform under study consists of two electromagnets M_{zl} and M_{zr} with μ_r = 6000 and area of pole-face equals to 4.05 mm^2 wounded with 700 turns of coil to levitate the platform. For each electromagnet poles, both equipped with an optical-sensor which is

manufactured by MTI Instrument with the probe having the capability of emitting a light to the surface and receiving the projection with a sensitivity of 0.868 *mm/V* and a linear range of 2 *mm* with a bandwidth of 140 *KHz* to measure its corresponding air gaps.
For each electromagnet poles, both equipped with an optical-sensor which is manufactured by MTI Instrument with the probe having the capability of emitting a light to the surface and receiving the projection with a sensitivity of 0.868 *mm/V* and a linear range of 2 *mm* with a bandwidth of 140 *KHz* to measure its corresponding air gaps. The signals were then send to a Pentium PC through a 12-bit high speed A/D converter with a conversion rate at 90K samples/sec and conversion range of ± 10 *volt*.

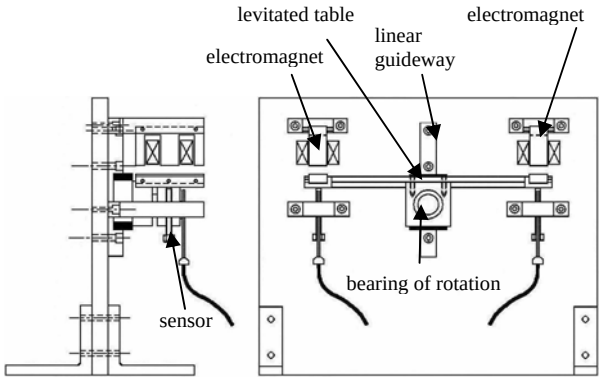

FIGURE 2: Schematic drawing of a two-DOF maglev platform

The control law was implemented using C-language at a sampling rate of 1*ms*.The control effort was then send out through a D/A converter with the conversion rate at 15 K samples/sec, and a range of 0 to 5 *volt* to a current source with current gain equals to 2 *A/V* with the maximum output of 2 *A* and a bandwidth of 10 *KHz* to drive the two electromagnets, M_{zl} and M_{zr} which levitated the platform thus closing the feedback loop.

The Dynamic Model of a 2-D.O.F Maglev

Assuming the mass center of the platform and its geometric center coincides, and it operates with small angular motions, the linearized equation of motion can thus be written as

$$\mathbf{H}\ddot{\mathbf{q}} = \mathbf{Q}$$
$$\mathbf{H} = \begin{bmatrix} M & 0 \\ 0 & I_{yy} \end{bmatrix},\ \mathbf{q} = \begin{bmatrix} z_c & \theta \end{bmatrix}^T \text{ and } \mathbf{Q} = \begin{bmatrix} F_z & \tau_{yy} \end{bmatrix}^T \tag{32}$$

Where M = 545±0.5g is the total mass of the levitated platform, while I_{yy} = 0.01915 *Kg-m*^{2} denotes the moment of inertia around the y-axis, respectively. z_c is the mass center moving in *z*-direction, and θ denotes the table's rotation in the z-direction. F_z and τ_{yy} are the electromagnetic force and torque exerting on the 2-D maglev. Let air gaps be z_l and z_r, respectively. And, $L = 199 \pm 0.5\,mm$ is the table length. The control force, f_l and f_r, on each side and torque generated by the two electromagnets are expressed as:

$$\begin{cases} f_l = \dfrac{\alpha I^2}{z_l^2} \\ f_r = \dfrac{\alpha I^2}{z_r^2} \\ F_z = f_l + f \\ \tau_{yy} = (f_r - f_l)L \end{cases} \tag{33}$$

with $\alpha = \dfrac{\mu_o N^2 A}{4}$.

Each optical sensor aligned with the center of the two electromagnets (M_{zl}, M_{zr}) can measure its corresponding air gaps. The linearized relationship between the displacement of the mass center (z_c) and pitch angle (θ) can be described as

$$\begin{cases} z_c = -\dfrac{z_l - z_r - w_z}{2} \\ \theta = -\dfrac{z_l - z_r}{L} \end{cases} \tag{34}$$

Because electromagnetic force and gravitational force are the external forces, the equations of motion can be expressed as

$$\begin{aligned} M\ddot{Z}_c &= F_Z - Mg + d_Z(t) \\ I_{yy}\ddot{\theta} &= \tau_{yy} + d_\theta(t) \end{aligned} \tag{35}$$

Where d_z and d_θ are lumped matched uncertainties. Moreover, based on the geometric relationship, the total electromagnetic forces f_l and f_r on two sides of the platform can be expressed in terms of F_z and τ_{yy}.

$$\begin{cases} f_l = \dfrac{1}{2}F_z - \dfrac{\tau_{yy}}{2L} \\ f_r = \dfrac{1}{2}F_z + \dfrac{\tau_{yy}}{2L} \end{cases} \tag{36}$$

Experimental Studies

Experiments were performed to verify the proposed scheme. In this sub-section, MSMC schemes utilize mode-switching between SMC and ISMC with fixed and state-dependent boundary layer were performed for comparison. It is also noted that the state-dependent boundary layer is determined based on a disturbance observer as described in the previous section.

Case 1: *The effect of controller selection*

From Fig. 3 and Fig. 4, SMC can obtain satisfactory settling time, while it enters the boundary layer, there exists a significant steady-state error, however. It is noted that while entering the switching region which is set at t=0.05 sec, ISMC has demonstrated its efficacy in reducing the steady state error, but it requires longer settling time and larger overshoot that will inevitably cause integral wind-up. It is seen that the response in pitch angle experienced a much violent vibration than that of vertical displacement. The mode-switching sliding mode(MSMC) has demonstrated its capability in the application on this Maglev platform but with the price of the fine tuning of proper switching region.

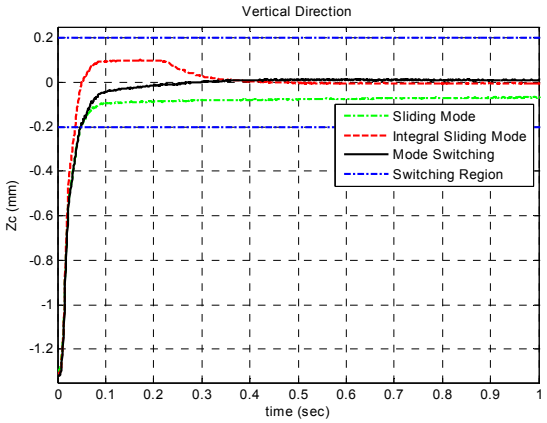

FIGURE 3: Response in Z-direction with different controllers

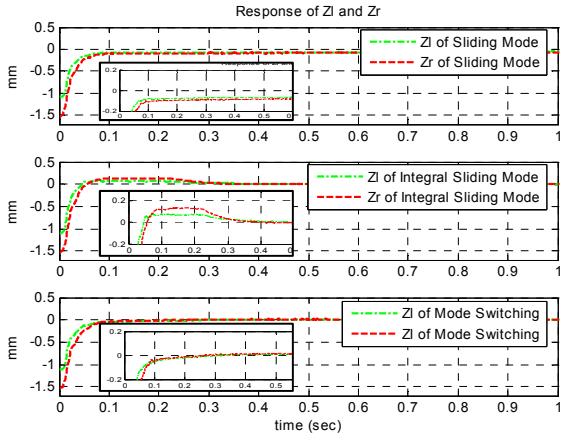

FIGURE 4: Response of left- and right-tip with different controllers

Case 2: *The effect of boundary layer selection*

Here, the MSMC is set to satisfy fixed switching instant, t_s=0.04 sec, but different boundary layers to investigate its effect on the control performance. The MSMC controller is designed to switch between a SMC and ISMC under pre-specified condition and its corresponding control parameters are listed as follows.

1. $\left|\tilde{Z}_c(0.04)\right| \le 0.1mm$, λ_z=64.164 sec^{-1}, λ_{zl}=32.083 sec^{-1}.
2. $\left|\tilde{Z}_c(0.04)\right| \le 0.2mm$, λ_z=46.835 sec^{-1}, λ_{zl}=23.418 sec^{-1}.
3. $\left|\tilde{Z}_c(0.04)\right| \le 0.3mm$, λ_z=36.699 sec^{-1}, λ_{zl}=18.350 sec^{-1}.

Where Z_c were calculated using Eq. (34) that combines Z_l with Z_r.

It can be seen from the experimental results as shown in Fig. 5 and Fig. 6 that if the boundary layer is set at $\left|\tilde{Z}_c\right| \le 0.2mm$. It could have the best performance among the three conditions in term of overshoot and steady state error. Moreover, the responses of left- and right-tip further revealed the efficacy of the MSMC scheme. Consequently, the mode-switching sliding mode has demonstrated its capability in the application on this Maglev platform provided that a fine tuning of proper boundary layer is needed.

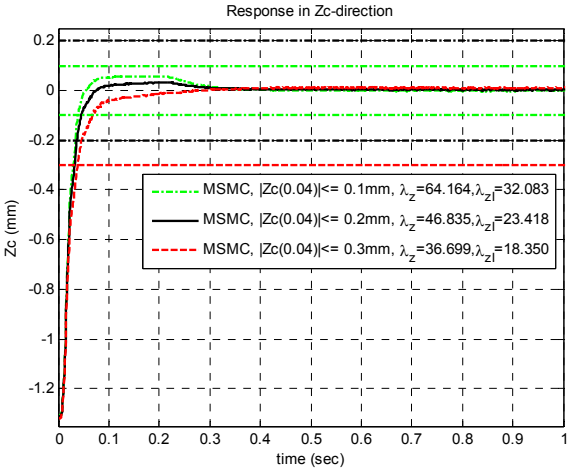

FIGURE 5: Response in *Z*-direction with different boundary layer

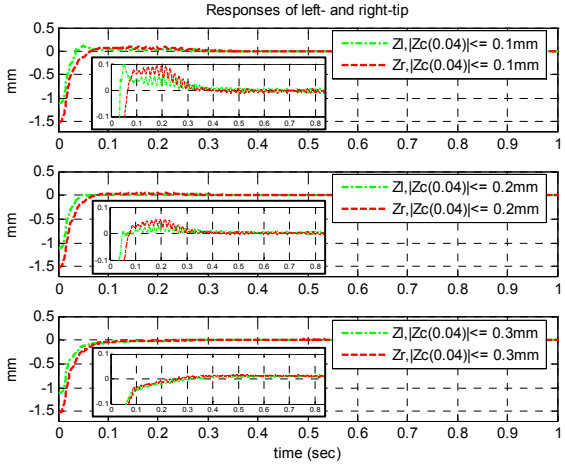

FIGURE 6: Responses of left- and right-tip with different boundary layer

Case 3: *The effect of switching time selection*

Here, the MSMC is set to satisfy different switching instant at fixed boundary layer, $\tilde{q}$ =0.2 *mm*, to investigate its effect on the control performance. The MSMC controller is designed to switch between a SMC and ISMC under pre-specified condition and its corresponding control parameters are listed as follows.

1. $\left|\tilde{Z}_c(0.06)\right| \le 0.2mm$, λ_z=31.223 sec^{-1}, λ_{zl}=15.612 sec^{-1}.
2. $\left|\tilde{Z}_c(0.05)\right| \le 0.2mm$, λ_z=37.467 sec^{-1}, λ_{zl}=18.734 sec^{-1}.
3. $\left|\tilde{Z}_c(0.04)\right| \le 0.2mm$, λ_z=46.835 sec^{-1}, λ_{zl}=23.418 sec^{-1}.

Where Z_c were calculated using Eq. (34) that combines Z_l with Z_r .

It can be seen from the experimental results as shown in Fig. 7 that if the switching instant is set at *t*=0.05 sec. It could have the best performance among the three conditions in terms of overshoot and steady state error. Furthermore, as shown in Fig. 8, the responses of left- and

right-tip further revealed the efficacy of the MSMC scheme. Consequently, the mode-switching sliding mode has demonstrated its capability in the application on this Maglev platform provided that a fine tuning of proper time is needed. It can be concluded from results of Case 1 and Case 2 that one can pre-specify $\left|\tilde{Z}_c\right| \le 0.2mm$ with switch instant at t=0.05 sec to have the best result among all tested conditions.

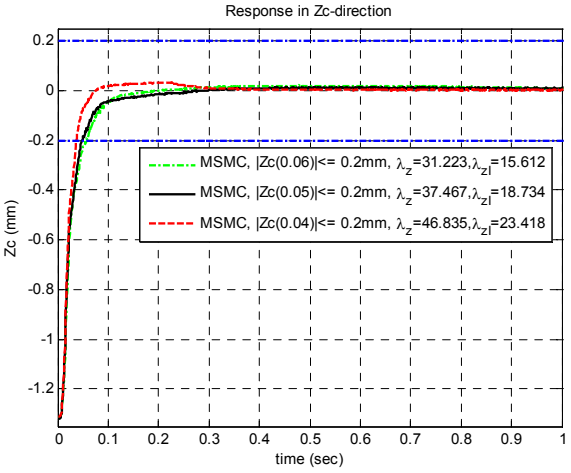

FIGURE 7: Response of in Z-direction with different switching time

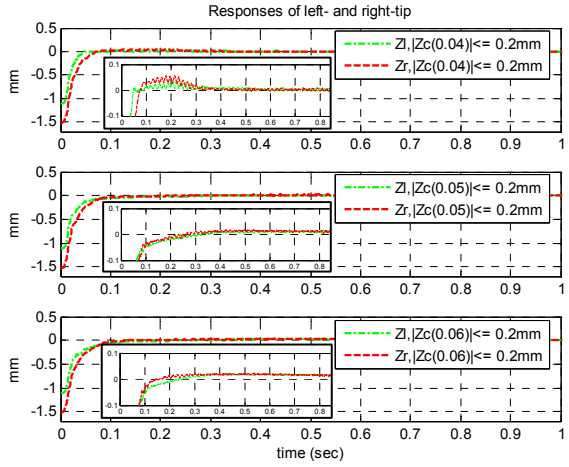

FIGURE 8: Responses of left- and right-tip with different switching time

Case 4: *MSMC with state-dependent boundary layer*

It is seen from the previous experimental results that we can select the switching region (in terms of layer thickness and switching instant) based on previous results through fining tuning process or engineering sense. As depicted in the previous section, a disturbance observer with state-dependent boundary layer for the on-line switching region selection for the MSMC scheme would perform the same result without trial and error. Finally, the experiments are performed to demonstrate its efficacy.

Test I: MSMC with state-dependent boundary layer controller under pre-specified condition and its

on-line switching region selection are listed as follows.

1. $\left|\tilde{Z}_c(0.04)\right| \le 0.1mm$, λ_z=64.164 sec^{-1}, λ_{zl}=32.083 sec^{-1}, K_{c1} =K_{c2} =320 sec^{-1}.
2. $\left|\tilde{Z}_c(0.05)\right| \le 0.2mm$, λ_z=37.467 sec^{-1}, λ_{zl}=18.734 sec^{-1}, K_{c1} =K_{c2} =187 sec^{-1}
3. $\left|\tilde{Z}_c(0.06)\right| \le 0.2mm$, λ_z=31.223 sec^{-1}, λ_{zl}=15.612 sec^{-1}, K_{c1} =K_{c2} =156 sec^{-1}

where K_{c1} and K_{c2} is based on the uncertain bounds of system in Eq.(30) and Eq.(31), respectively.

As shown in Fig. 9, the state-trajectory of vertical displacement would be constrained inside the state-dependent boundary layer as expected. On the other hand, the tips' responses are also shown in Fig. 10. Obviously, the different gaps of left- and right-tip have been estimated and compensated on-line using the MSMC with state dependent boundary layer.

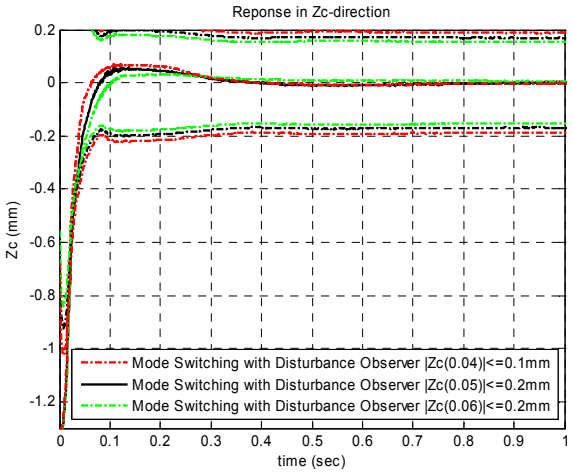

FIGURE 9: Responses in Z-direction with state dependent boundary layer

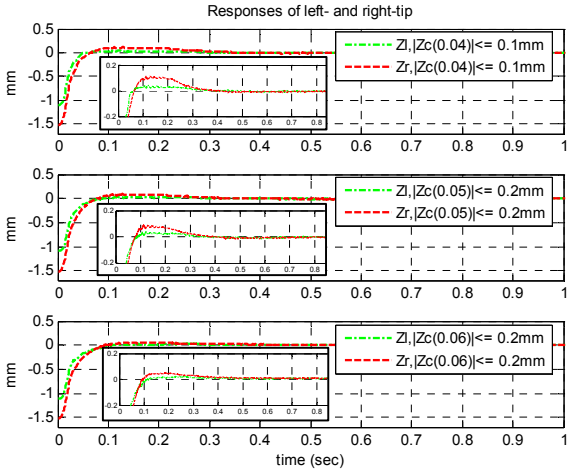

FIGURE 10: Responses in left- and right-tip with state dependent boundary layer

Test II: Compare with their counterparts in Case 1 and Case 2 with the same control laws and the same switching region,

$\left|\tilde{Z}_c(0.05)\right| \le 0.2mm$, λ_z=37.467 sec^{-1}, λ_{zl}=18.734 sec^{-1}, K_{c1} =K_{c2} =187 sec^{-1}

As Fig. 11 and Fig. 12 show, the experimental result on vertical direction is seen to be equipped with the augmented disturbance observer; a faster settling time and smaller steady-state error were achieved. It is also noted that the switching region is time-varying due to its state-dependent nature but is adjusted on-line based on the estimated result from the augmented disturbance observer.

Consequently, MSMC with state-dependent boundary layer have the best performance among the four conditions in terms of smoothness, overshoot and steady state error.

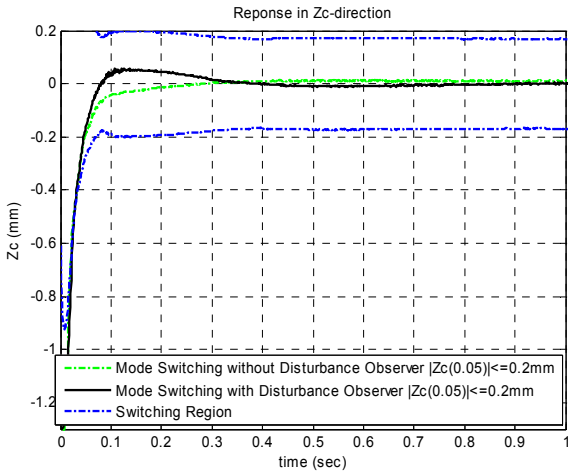

FIGURE 11: Responses in *Z*-direction with state dependent boundary layer

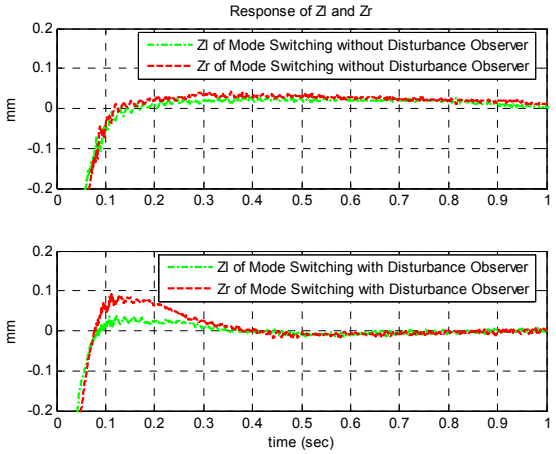

FIGURE 12: Responses in left- and right-tip with state dependent boundary layer

5. CONSLUSION

This paper presented a Mode-Switching Sliding-mode Control (MSMC) scheme that can switch between different sliding-mode control schemes. Switching would occur while the states entering the vicinity of a preset operating point. MSMC can provide better positioning performance than SMC and ISMC alone. The proposed state-dependent boundary layer based-on a disturbance observer can not only precisely compensate for system perturbation within the pre-specified

frequency range, but also reduce the adverse effect due to chattering. MSMC with disturbance observer using state-dependent boundary layer design has been successful applied to a two-DOF Maglev platform. The experiment results also showed that the maglev system can track the reference input within the pre-specified errors, i.e. $\tilde{Z}_c$ and $\tilde{\theta}$ as expected, and it can also provide certain robust performance for systems subjected to uncertainties from both parameters and external disturbance with an auto-tuned switching region based on a state-dependent boundary layer incorporated with disturbance observer design.

6. REFERENCES

1. K. D. Young, V. I. Utkin and U. Ozguner. *"A control engineer's guide to sliding model control".* IEEE Trans. on Control System Technology, 7(3):328-342, 1999
2. J. J. E. Slotine and W. Li. *"Applied Nonlinear Control*, Prentice-Hall", New Jersey, pp. 276-310(1991)
3. Utkin, Jurgen Guldner and Jingxin Shi. *"Sliding Mode Control in Electromechanical Systems"*, CRC Press, pp. 131-153(1999)
4. J. J. E. Slotine and S. S. Sastry. "*Tracking control of non-liner systems using sliding surface, with application to robot manipulators".* Int. J. of Control, 38(2):465-492, 1983
5. B. W. Bekit, J. F. Whidborne and L. D. Seneviratne, "*Sliding mode control for robot manipulators using time-varying switching gain and boundary layer".* Control '98. UKACC International Conference on, London, United Kingdom, 1998.
6. M. -S. Chen, Y. R. Hwang and M. Tomizuka. "*A state-dependent boundary layer design for sliding mode control".* IEEE Trans. on Automatic Control, 47(10):1677-1681, 2002
7. M. -S. Chen, Y. R. Hwang and M. Tomizuka, "*Sliding mode control reduced chattering for systems with dependent uncertainties".* Networking, Sensing and Control, 2004 IEEE International Conference on, Taipei, Taiwan, 2004
8. M. Iwasaki, K. Sakai and N. Matsui, *"High-speed and high-precision table positioning system by using mode switching control".* Industrial Electronics Society, 1998. IECON '98. Proceedings of the 24th Annual Conference of the IEEE**,** Nagoya, Japan 1998.
9. T. Yamaguchi, H. Numasato, H. Hirai, "*A mode-switching control for motion control and its application to disk drives: design of optimal mode-switching conditions".* IEEE/ASME Trans. on Mechatronics, 3(3):202-209, 1998
10. C. -Y. Hsu. "*Application of Switching Law to A 2-DOF Maglev Platform".* Master Thesis, National Tsing Hua University, June 2005
11. Y. -S. Lu and J. -S. Chen. "*Design of a perturbation estimator using the theory of variable-structure system and its application to magnetic levitation systems".* IEEE Trans. on Industrial Electronics, 43(3):281-289, 1995